Nanoscale

PAPER

View Article Online
View Journal | View Issue

Cite this: *Nanoscale*, 2022, **14**, 12849

Free-standing two-dimensional sheets of polymer-linked nanoparticles†

Xiaole Hu, Ji-eun Park, Seulki Kang, Chan-Jin Kim, Youngji Kim, Jerome Kartham Hyun and So-Jung Park *

Received 20th June 2022,
Accepted 11th August 2022

DOI: 10.1039/d2nr03375e

rsc.li/nanoscale

Here, we report a simple and general approach to fabricate free-standing two-dimensional (2D) sheets of nanoparticles by the simultaneous self-assembly of hydrophobic nanoparticles and hydrophilic polymers at the liquid–liquid interface. The nanoparticle–polymer interaction at the interface generates well-defined 2D sheets of densely packed nanoparticles with a lateral dimension of tens of micrometers. The nanosheets transferred in water are stable over months without any additional cross-linking step. The method is applicable for a broad range of nanoparticles including oxide, semiconductor, and metal nanoparticles as well as functional polymers.

Introduction

Two-dimensional (2D) assemblies of nanoparticles are of great interest as they possess structural features and physical properties useful for various applications.[1–7] For example, 2D superlattices of metal, semiconductor, and magnetic nanoparticles have been used as model systems to investigate charge and spin transport in nanoparticle assemblies;[8] composite membranes of nanoparticles and polymers were used to construct highly sensitive sensor arrays;[1] and 2D assemblies of metal nanoparticles can serve as excellent substrates for surface enhanced Raman spectroscopy (SERS).[9,10]

Various wet and dry methods have been reported for the preparation of traditional 2D materials such as graphene and transition metal dichalcogenides. In particular, the development of solution-processible chemical methods has significantly broadened the scope of their applications.[11] 2D assemblies of nanoparticles are usually prepared by a drying process[12,13] or by self-assembly at a liquid interface followed by transfer to a solid substrate.[8,14,15] Only a small number of effective approaches has been reported to date for the fabrication of free-standing and solution-processible 2D films of nanoparticles.[16,17] Russell and coworkers have reported that nanoparticles adsorb on the surface of emulsion droplets to reduce the interfacial energy between two immiscible liquids, which can be covalently crosslinked to form an ultrathin QD membrane.[18,19] We have reported emulsion-based self-assembly of nanoparticles, forming well-defined vesicle-like assemblies with internal structures controllable by the type of surfactants.[20] In a related study, Tan and coworkers recently prepared free-standing nanoparticle sheets with the introduction of a cocktail of surfactants.[21]

Here, we report a simple solution-phase approach for the fabrication of free-standing 2D assemblies of nanoparticles based on simultaneous self-assembly of nanoparticles and polymers at the liquid–liquid interface. Through the self-assembly, hydrophobic inorganic nanoparticles are transferred into water as free-standing 2D sheets that are stable over months without any additional cross-linking step. Our approach is general and can be applied to various types of nanoparticles such as iron oxide, metal, and semiconductor nanoparticles when coupled with a suitable polymer.

Department of Chemistry and Nanoscience, Ewha Womans University, 52 Ewhayeodae-gil, Seodaemun-gu, Seoul, 03760, Korea.
E-mail: sojungpark@ewha.ac.kr

†Electronic supplementary information (ESI) available: Materials and instrumentation, detailed synthetic procedure and characterization data (TEM, UV-vis and PL spectroscopy) for nanoparticles (IONPs, AuNPs), characterization (TEM, PL) of semiconductor nanoparticles (QDs, QRs), characterization data of PAA (GPC, ^{1}H NMR, and FT-IR), magnetic attraction test of IONP (5.2 nm)/PAA_{69} nanosheets, stability test of nanosheets, the effect of pH, nanoparticle concentration, and polymer type and concentration on the nanosheet formation, TEM and optical microscope images of metal nanoparticle/PEDOT:PSS nanosheets. See DOI: https://doi.org/10.1039/d2nr03375e

Results and discussion

Self-assembly of iron oxide nanoparticles (IONPs) into 2D nanosheets

In a typical procedure, a chloroform containing oleic acid-stabilized IONPs and an aqueous solution of poly(acrylic acid) (PAA_{69}) were mixed in a vial with vigorous stirring overnight (Fig. 1A). Here, PAA was selected for its affinity to metal oxide surfaces.[22] This procedure results in the transfer of hydrophobic IONPs from the chloroform to the aqueous phase, as

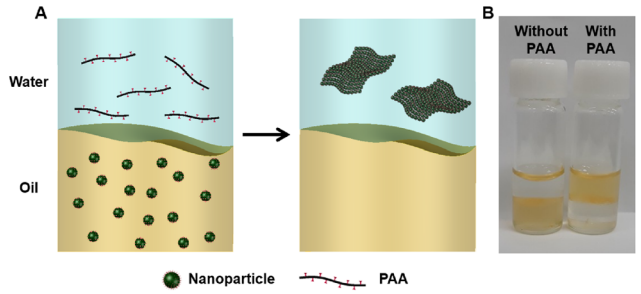

Fig. 1 (A) Schematic illustration of self-assembly of IONP and PAA into 2D structures. (B) Photograph showing the transfer of 5.2 nm IONPs from the bottom chloroform layer to the top water layer in the presence of PAA.

evidenced by the yellow coloration of the top aqueous phase (Fig. 1B). A control experiment was performed without PAA, which showed no significant transfer of nanoparticles to the water layer (Fig. 1B).

The aqueous phase containing nanoparticles was slightly opaque, indicating that nanoparticles are transferred as a type of assemblies rather than isolated particles. The nanoparticle assemblies dispersed in water could be collected by a magnet due to the collective response of magnetic nanoparticles in the assemblies to the magnetic field (Fig. S6†). The transferred nanoparticle assemblies were collected by light centrifugation (5000 rpm, 5 min), and redispersed in water for further characterization.

Interestingly, transmission electron microscope (TEM) and atomic force microscope (AFM) images revealed that nanoparticles form unique 2D assemblies. Fig. 2 presents TEM and AFM images of nanosheets prepared from three different size IONPs (5.2 ± 0.4 nm, 9.5 ± 0.8 nm, 14 ± 0.7 nm). For all three cases, nanoparticles assemble into large nanosheets in the size range of tens of micrometers (Fig. 2A, D and G), which are made up of densely packed nanoparticles (Fig. 2B, E and H). The result indicates that the self-assembly mechanism operates for a broad range of nanoparticle sizes. The thicknesses of nanosheets were measured to be 16 ± 1 nm, 18 ± 1 nm, 22 ± 1 nm for nanosheets made of 5.2 nm, 9.5 nm, and 14 nm IONPs (Fig. 2C, F and I), indicating that the nanosheets are mostly composed of one to a few layers of nanoparticles. The 2D nanosheets were stable over a year without any additional crosslinking step (Fig. S7†).

Self-assembly of quantum dots (QDs) into 2D nanosheets

As the carboxylic acid functional group has the affinity to various types of inorganic materials including metal oxides and chalcogenides,[22–24] we introduced QDs and quantum rods (QRs) for the 2D self-assembly. Fig. 3A, B, D and E presents TEM images of self-assembled nanostructures from octadecylamine-stabilized QDs (*i.e.*, 3.2 ± 0.5 nm CdSe, 15 ± 1 nm CdSe/CdS) and PAA_{243}, which show large 2D sheets composed of densely packed QDs. Fluorescence microscope images reveal green- and red-fluorescent nanosheets for CdSe and

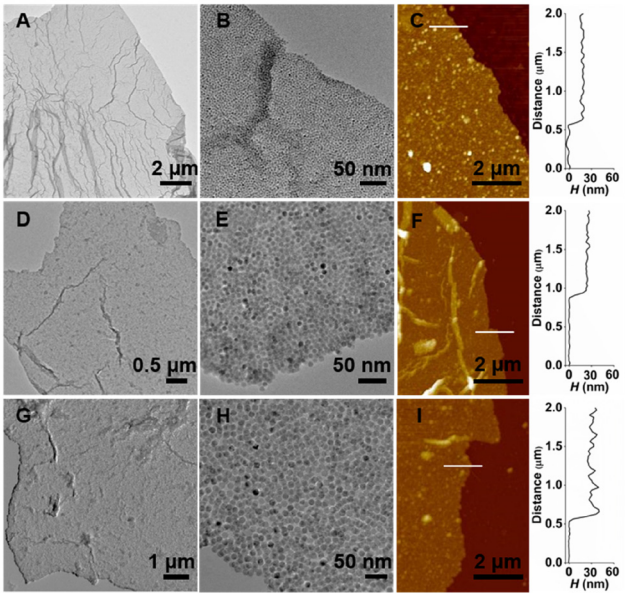

Fig. 2 2D sheets of IONP of varying diameters formed with PAA_{69}. (A and B) TEM images of nanosheets made of 5.2 nm IONP. (C) AFM image and height (*H*) profile of nanosheets made of 5.2 nm IONP. (D and E) TEM images of nanosheets made of 9.5 nm IONP. (F) AFM image and *H* profile of nanosheets made of 9.5 nm. (G and H) TEM images of nanosheets made of 14 nm IONP. (I) AFM image and *H* profile of nanosheets made of 14 nm IONP.

CdSe/CdS QDs (Fig. 3C and F), respectively, consistent with their photoluminescence spectra (Fig. S2F†). The self-assembly was further extended to a rod-shaped particle, trioctylphosphine oxide-stabilized CdSe/CdS QRs (width: 5.2 ± 0.7 nm, length: 58 ± 9 nm), which again formed large red-fluorescent nanosheets of densely packed QRs in the presence of PAA_{243} (Fig. 3G–I).

Mechanism behind the formation of 2D nanosheets

Liquid–liquid interfaces can serve as soft templates for 2D assembly of nanoparticles, as the interfacial energy between dissimilar liquids induces adsorption of nanoparticles at the interface.[19] Such nanoparticle adsorption is a dynamic process and nanoparticles can come on and off of the interface and laterally mobile at the initial stage of self-assembly where the nanoparticle density is low.[14] In our self-assembly, both the nanoparticles in the oil phase and the polymers in the aqueous phase can adsorb onto the oil–water interface, acting as surfactants.[19] PAA can then bind to the surface of IONPs at the interface through the bidentate metal binding of carboxylates.[25] The multivalency effect of many carboxylic acid groups on PAA can facilitate the replacement of oleic acid on IONPs.[26] Once hydrophilic PAA strands partially bind onto a hydrophobic nanoparticle, they together can act as a better hybrid surfactant composed of hydrophobic and hydrophilic parts (Scheme 1). In addition, PAA strands can crosslink nanoparticles at the interface at the later stage of self-assembly where the nanoparticle density becomes high enough

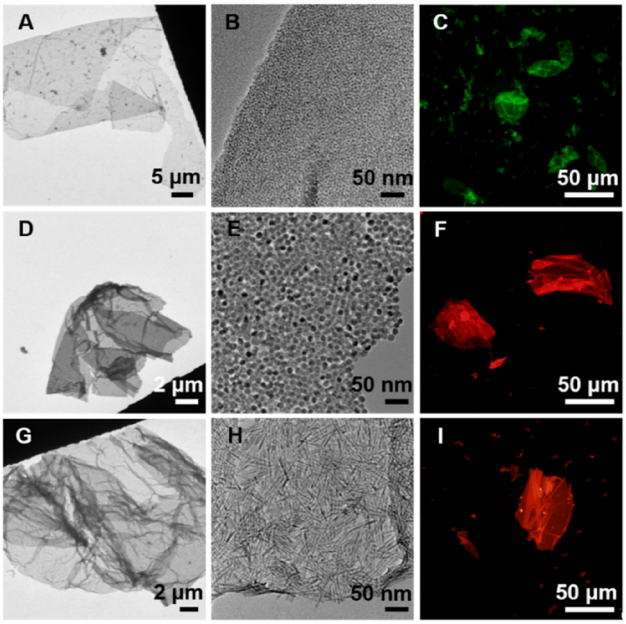

Fig. 3 2D sheets of CdSe and CdSe/CdS quantum dots and CdSe/CdS QDs quantum rods formed with PAA_{243}. (A–C) TEM (A and B) and fluorescent microscope (C) image of 2D sheets made of 3.2 nm CdSe QDs. The fluorescent image was taken with the excitation filter of λ_{ex} = 450–480 nm and the emission filter of λ_{em} = 515 nm. (D–F) TEM (D and E) and fluorescent microscope (F) image of 2D sheets made of 15 nm CdSe/CdS QDs. The fluorescent image was taken with excitation filter of λ_{ex} = 510–550 nm and emission filter of λ_{em} = 590 nm. (G–I) TEM (G and H) and fluorescent microscope (I) image of 2D sheets made of QRs (width 5.2 nm, length 58 nm). The fluorescent image was taken with excitation filter of λ_{ex} = 510–550 nm and emission filter of λ_{em} = 590 nm.

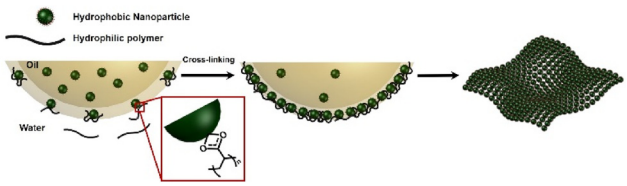

Scheme 1 Schematic illustration showing the mechanism behind the 2D self-assembly.

(Scheme 1). Finally, 2D sheets of nanoparticles cross-linked with hydrophilic PAA can escape from the interface with agitation and are transferred into the water layer.

To test the hypothesis, we examined how the factors related to PAA affect the self-assembly. Firstly, in the absence of PAA, no self-assembly or nanoparticle transfer was observed (Fig. 1B). In addition, when the amount of polymers relative to that of nanoparticles is too small, significant amounts of nanoparticles remain in the chloroform phase (Fig. S8 and S9†). These results indicate that PAA is necessary for the formation and transfer of 2D assemblies of nanoparticles. Secondly, PAA with a higher molecular weight was more effective for the 2D assembly and transfer of large nanoparticles. The polymer length effect was investigated with 15 nm QDs and three different length polymers, PAA_{30}, PAA_{65}, and PAA_{243}. Shorter polymers (*i.e.*, PAA_{30}, PAA_{65}) induced accumulation of 15 nm QDs at the liquid–liquid interface. However, they remained at the interface even with vigorous agitation (Fig. S10†). On the contrary, the longest polymer, PAA_{243} generated stable free-standing 2D assemblies of QDs in water, as shown in Fig. 3. Thirdly, three-dimensional (3D) irregular aggregates were predominantly formed at pH 1.8 and 3.4 (Fig. S11A and B†) in contrast to the large ultrathin 2D nanosheets formed at pH > 4.5 (Fig. S11C and D†). This behaviour can be explained by the pH-dependent charge state, binding efficiency, and conformation of PAA. Deprotonated carboxylate at pH > 4.5 can bind to metal oxides more strongly than protonated carboxylic acid due to the chelating effect.[25] The deprotonation also induces conformational changes of PAA from the globule to extended state. Deprotonated PAA can bind to multiple nanoparticles in its extended state, which can promote the formation of large 2D assemblies. In addition, negatively charged PAA at pH > 4.5 should improve solvation of nanosheets in water, leading to high transfer efficiency to water. On the contrary, 3D aggregates of nanoparticles are formed in an acidic condition due to limited water solubility and metal binding efficiency of PAA in its protonated form.[27]

To investigate the importance of nanoparticle–polymer interactions, we employed two other hydrophilic polymers, poly(ethylene oxide) (PEO, 60 000 g mol^{-1}) and poly(vinyl alcohol) (PVA, 9000–10 000 g mol^{-1}) for the interfacial self-assembly of IONPs. These polymers can also transfer nanoparticles into the water layer, but in the form of 3D aggregates or thicker films rather than well-defined 2D sheets (Fig. S12†). These observations indicate that the polymer–nanoparticle and polymer–polymer interactions play important roles for the formation of nanosheets, and are consistent with our hypothesis described above.

Extending 2D self-assembly to other polymer–nanoparticle pairs

To further test our hypothesis, we adopted another prototypical polymer, poly(acrylamide) ($PAAm_{3486}$, 150 000 g mol^{-1}) for gold nanoparticles (AuNPs) stabilized with oleylamine, taking advantage of the interaction between amine groups and AuNPs.[28,29] Consistent with our hypothesis, nanosheets made of AuNPs (5.2 ± 0.4 nm) were obtained with $PAAm_{3486}$, as presented in Fig. 4A and B. The red-shift and dampening of the surface plasmon resonance band is consistent with the formation of densely packed nanoparticle assemblies (Fig. 4C). PAAm was broadly applicable for IONPs (5.2 nm, Fig. 4D and E) and QDs (15 nm, Fig. 4G and H) as well as metal nanoparticles, since the amine group also interacts with metal oxides and chalcogenides.[29] The magnetic manipulation (Fig. 4F) and fluorescent optical microscope imaging (Fig. 4I) confirmed the presence of IONPs and QDs in the respective nanosheets.

In addition to prototypical polymers used above, a functional polymer, poly(3,4-ethylenedioxythiophene)-polystyrene

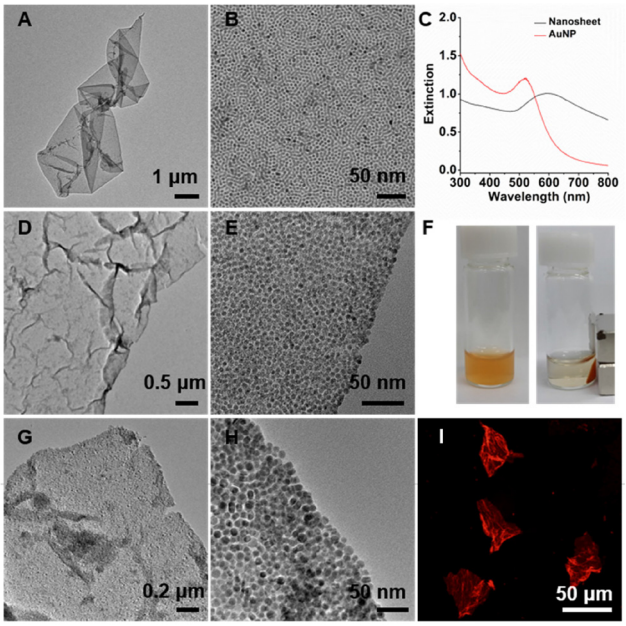

Fig. 4 Extending the self-assembly to $PAAm_{3486}$ with three different nanoparticles. (A–C) TEM images (A and B) and extinction spectra (C) of 2D sheets made of 5.2 nm AuNPs. An extinction spectrum of dispersed AuNPs is also provided for comparison. (D–F) TEM images (D and E) and a photograph showing magnetic attraction of 2D sheets made of 5.2 nm IONPs (G–I) TEM images (G and H) and a fluorescent microscope image (I) of 2D sheets made of 15 nm QDs. The fluorescent image was taken with excitation filter of λ_{ex} = 510–550 nm and emission filter of λ_{em} = 590 nm.

sulfonate (PEDOT:PSS) was introduced for 2D self-assembly of QDs. PEDOT:PSS is one of the most widely used commercial conducting polymer, composed of conductive PEDOT and negatively charged PSS, which can bind to metal and metal chalcogenides.[30,31] As presented in Fig. 5, well-defined 2D assemblies of QDs and PEDOT:PSS were formed and transferred into the water phase.

Multicomponent nanosheets

As one type of polymer can interact with nanoparticles of different compositions, sizes and shape, the 2D self-assembly can be extended to fabricate multifunctional nanosheets composed of different types of nanoparticles. Three different polymers, PAA_{243}, $PAAm_{3486}$, and poly(sodium 4-styrenesulfonate) (PSS_{343}, ~70 000 g mol^{-1}) containing carboxylic acid, primary amine, and sulfonate functional groups were adopted for the binary self-assembly of 15 nm QD/5.2 nm IONP (Fig. 6A and B), 5.2 nm AuNP/5.2 nm IONP (Fig. 6C and D), and 5.2 nm AuNP/15 nm QD (Fig. 6E and F) pairs, respectively (Fig. 6). In all three cases, well-defined binary 2D sheets composed of densely packed nanoparticles were observed, confirming our hypothesis.

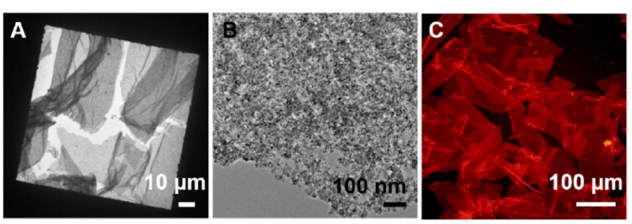

Fig. 5 2D self-assembly of PEDOT:PSS and QDs. TEM (A and B) and optical microscope images (C) of 2D sheets made of 15 nm QD and PEDOT:PSS.

Surface-enhanced Raman scattering (SERS) on nanosheets

Nanosheets of plasmonic particles can serve as excellent substrates for SERS due to their large surface area and ability to sustain highly enhanced near fields over the numerous interparticle junctions. To test this capability, SERS measurements were carried out on nanosheets prepared with 5.2 nm AuNPs and PAAm (Fig. 4), using rhodamine B (RB) as the probe molecule. As presented in Fig. 7A, strong RB Raman signals were observed at 621 cm^{-1} (xanthene ring puckering mode), 1199 and 1277 cm^{-1} (C–C bridge band stretching and aromatic C–H bending), 1358 cm^{-1} (aromatic C–C bending), 1509 and 1531 cm^{-1} (aromatic C–H bending), and 1647 cm^{-1} (aromatic C–C bending and C=C stretching) for AuNP/PAAm nanosheets.[32] The RB Raman signal was barely observed in the control experiment carried out with AuNPs dried on a silicon substrate, which is composed of isolated AuNPs and irregular aggregates. Fig. 7B presents the intensity histogram for nanosheet and control samples at 612 cm^{-1}, which clearly shows that the average intensity on nanosheets was significantly higher than that on the control sample. The strong Raman signal from nanosheets is attributed to the highly accessible large number of regularly placed field-enhancement

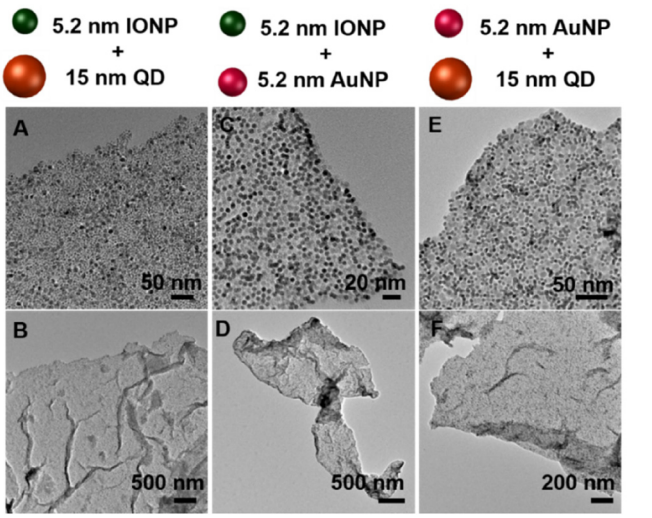

Fig. 6 Binary 2D sheets. (A and B) TEM images of binary 2D sheets made of 5.2 nm AuNP and 15 nm QD with PAA_{243}. (C and D) TEM images of binary 2D sheets made of 5.2 nm IONP and 5.2 nm AuNP with $PAAm_{3486}$. (E and F) TEM images of binary 2D sheets made of 5.2 nm AuNP and 15 nm QD with PSS_{343}.

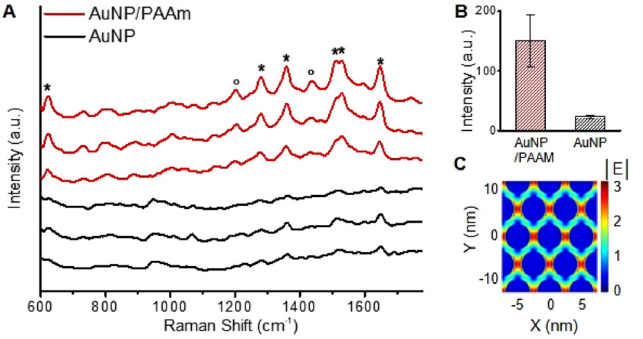

Fig. 7 (A) SERS spectra of RB on the AuNP/PAAm nanosheet and the control sample prepared by drying AuNPs on a silicon substrate with the excitation wavelength of 633 nm. Symbols, * and ○ indicate characteristic Raman peaks of RB and PAAm, respectively. (B) Average Raman intensity of RB on AuNP/PAAm nanosheets (red) and the control sample (black) at 621 cm^{-1}. (C) Near-field electric field distribution on a 5.2 nm AuNP array on a silicon substrate under the illumination of *x*-polarized 633 nm incident light.

sites. Fig. 7C presents simulated electric field distribution in a 2D array of AuNPs, modelled using experimental parameters obtained from TEM images (*i.e.*, AuNP diameter of 5.2 nm, junction size of 1.4 nm), under the illumination of *x*-polarized 633 nm incident light. A field map for a single AuNP is also presented in Fig. S13† for comparison. The simulated results show that the field intensity is highly enhanced for the nanosheet compared to that of a single AuNP even for the small size AuNPs, consistent with the SERS results.

Conclusion

In summary, we have developed a simple approach to fabricate free-standing 2D sheets of nanoparticles based on the self-assembly of nanoparticles and polymers at the liquid–liquid interface. The nanosheets are typically in the size range of tens of micrometers, and mostly composed of monolayers of densely packed nanoparticles. In this approach, as-synthesized hydrophobic nanoparticles in the organic phase and hydrophilic polymers in water simultaneously adsorb at the interface. The nanoparticle–polymer interaction at the interface generates large 2D sheets of nanoparticles that are stable over a year without any additional crosslinking step. While there has been active investigation on polymer nanocomposite materials, a majority of studies concerned isotropic assemblies where a large fraction of nanoparticles is buried inside the assemblies.[33] 2D assembly structures reported here are of particular interest, as most nanoparticles in the assemblies are exposed to the environment, which is useful for various applications such as sensors and catalysts. Furthermore, the resulting assemblies are dispersed in water, which is advantageous for further materials processing. This method is generally applicable for a broad range of nanoparticles including oxide, compound semiconductor, and metal particles of varying sizes and shapes when paired with proper polymers. We have demonstrated the formation of 2D sheets of IONPs, QDs, QRs, AuNPs, and their mixtures using PAA, PAAm, and PSS. Furthermore, a conducting polymer can be adopted to fabricate hybrid 2D nanosheets with added functionalities.

Experimental method

Synthesis and characterization of nanoparticles and polymers

IONPs with varying diameters (5.2 ± 0.4 nm, 9.5 ± 0.8 nm, 14 ± 0.7 nm),[34] CdSe (3.2 ± 0.5 nm) QDs,[35] CdSe/CdS core/shell QDs (15 ± 1 nm),[35,36] CdSe/CdS core/shell QRs (length: 5.2 ± 0.7 nm, width: 58 ± 9 nm),[35,37] and gold (AuNPs, 5.2 ± 0.4 nm) were synthesized by well-established literature procedures. PAA was prepared by the hydrolysis of poly(*tert*-butyl acrylate) (PtBA) synthesized by the reversible addition–fragmentation chain-transfer (RAFT) polymerization, following a previously reported method.[26] Other polymers were purchased from Sigma-Aldrich and used as received. The characterization data of synthesized nanoparticles (Fig. S1–S3†) and polymers (Fig. S4 and S5†) are provided in the ESI.†

Self-assembly of IONP and PAA_{69}

In typical experiments, IONPs (0.2 mg mL^{-1}, 1 mL) in chloroform was added to an aqueous solution of PAA_{69} (1.5 mg mL^{-1}, 1 mL) in a 5 mL glass vial, which was stirred at 1200 rpm at ambient temperature overnight. The pH of PAA stock solution was adjusted to pH 7.0 by using 1 M sodium hydroxide (NaOH) or 1 M hydrochloric acid (HCl) solution. After vigorously stirring overnight, the water phase was taken into a microtube. Then, the nanosheets dispersed in the aqueous phase were collected by centrifugation (5000 rpm, 5 min) and resuspended in 1 mL water for further characterization. The same procedure was used for the self-assembly of QD and QR.

Self-assembly of AuNPs and $PAAm_{3486}$

$PAAm_{3486}$ (150 000 g mol^{-1}) was purchased from the Sigma-Aldrich and used without any further treatment. An aqueous solution of $PAAm_{3486}$ (6 mg mL^{-1}, 1 mL) was added to AuNP solution (5.2 nm, 1 mL chloroform) in a 5 mL glass vial, which was stirred at 1200 rpm at ambient temperature for overnight. After vigorous overnight stirring, the organic phase became colorless and the water phase became blue-colored due to the formation of nanoparticle assemblies. The nanosheets in the aqueous phase were collected by centrifugation (5000 rpm, 5 min) and resuspended in 1 mL water for further characterization. The same procedure was used for IONPs (5.2 nm) and QDs (15 nm).

Self-assembly of PEDOT:PSS and QD

PEDOT:PSS (1.0 wt% in water) was purchased from the Sigma-Aldrich and used without any further treatment. In a typical experiment, QD solution (15 nm, 0.5 mg mL^{-1}, 1 mL chloroform) was added to the polymer solution (0.025 wt% in water, 1 mL) in a 5 mL glass vial equipped with a stirring bar. After vigorous overnight stirring, the water phase containing QD/

PEDOT:PSS sheets was transferred into a microtube. The nanosheets were collected by centrifugation (5000 rpm, 5 min) and redispersed in 1 mL water for characterization.

SERS measurements

In typical experiments, 10 μL of nanosheets or AuNPs in solution (AuNP concentration: 100 nM) were placed on a silicon wafer and dried under the ambient condition for several hours. 5 μL of aqueous RB (2 μM) solution was placed on the substrate and dried overnight. SERS measurements were carried out on a micro-Raman spectrometer with a 633 nm laser.

Conflicts of interest

The authors declare no competing financial interest.

Acknowledgements

This work was supported by the National Research Foundation of Korea (NRF) grant funded by the Korea government (MSIP) (NRF-2018R1A2B3001049, NRF-2017R1A5A1015365) and by the Basic Science Research Program through the National Research Foundation of Korea (NRF) funded by the Ministry of Education (NRF-2019R1I1A1A01044158) (J.-e. P.). Electron microscope imaging was carried out with the support from the Korea Basic Science Institute (National Research Facilities and Equipment Center) grant funded by the Ministry of Education (2020R1A6C101B194).

References

1 C. Jiang, S. Markutsya, Y. Pikus and V. V. Tsukruk, *Nat. Mater.*, 2004, **3**, 721–728.
2 P. Kanjanaboos, X. M. Lin, J. E. Sader, S. M. Rupich, H. M. Jaeger and J. R. Guest, *Nano Lett.*, 2013, **13**, 2158–2162.
3 J. Shen, B. Luan, H. Pei, Z. Yang, X. Zuo, G. Liu, J. Shi, L. Wang, R. Zhou, W. Cheng and C. Fan, *Adv. Mater.*, 2017, **29**, 1606796.
4 R. Cai, D. Yang, L. Yan, F. Tian, J. Zhang, Y. Lyu, K. Chen, C. Hong, X. Chen, Y. Zhao, Z. Chen and W. Tan, *ACS Appl. Nano Mater.*, 2018, **1**, 5389–5395.
5 R. Cai, Y. Du, D. Yang, G. Jia, B. Zhu, B. Chen, Y. Lyu, K. Chen, D. Chen, W. Chen, L. Yang, Y. Zhao, Z. Chen and W. Tan, *Nanoscale*, 2019, **11**, 12169–12176.
6 M. Cao, Y. Damji, C. Zhang, L. Wu, Q. Zhong, P. Li, D. Yang, Y. Xu and Q. Zhang, *Small Methods*, 2020, **4**, 2000303.
7 C. Huang, Z. Guo, X. Zheng, X. Chen, Z. Xue, S. Zhang, X. Li, B. Guan, X. Li, G. Hu and T. Wang, *J. Am. Chem. Soc.*, 2020, **142**, 9408–9414.
8 A. Dong, J. Chen, P. M. Vora, J. M. Kikkawa and C. B. Murray, *Nature*, 2010, **466**, 474–477.
9 Y. H. Lee, W. Shi, H. K. Lee, R. Jiang, I. Y. Phang, Y. Cui, L. Isa, Y. Yang, J. Wang, S. Li and X. Y. Ling, *Nat. Commun.*, 2015, **6**, 6990.
10 Y. Shin, J. Song, D. Kim and T. Kang, *Adv. Mater.*, 2015, **27**, 4344–4350.
11 Q. Shi and W. Cheng, *Adv. Funct. Mater.*, 2020, **30**, 1902301.
12 J. Lee, G. Bhak, J. H. Lee, W. Park, M. Lee, D. Lee, N. L. Jeon, D. H. Jeong, K. Char and S. R. Paik, *Angew. Chem., Int. Ed*, 2015, **54**, 4571–4576.
13 Y. Liu, B. Fan, Q. Shi, D. Dong, S. Gong, B. Zhu, R. Fu, S. H. Thang and W. Cheng, *ACS Nano*, 2019, **13**, 6760–6769.
14 F. Reincke, S. G. Hickey, W. K. Kegel and D. Vanmaekelbergh, *Angew. Chem., Int. Ed.*, 2004, **43**, 458–462.
15 S. Oh, M. Yang, S. Kang, S. H. Chung, J. Bouffard, S. Hong and S. J. Park, *ACS Appl. Mater. Interfaces*, 2019, **11**, 28538–28545.
16 Z. Tang, Z. Zhang, Y. Wang, S. C. Glotzer and N. A. Kotov, *Science*, 2006, **314**, 274–278.
17 F. G. Xu, P. F. Zhang, J. C. Zhang, C. Y. Yu, D. Y. Yan and Y. Y. Mai, *ACS Macro Lett.*, 2018, **7**, 1062–1067.
18 Y. Lin, H. Skaff, A. Boker, A. D. Dinsmore, T. Emrick and T. P. Russell, *J. Am. Chem. Soc.*, 2003, **125**, 12690–12691.
19 Y. Lin, H. Skaff, T. Emrick, A. D. Dinsmore and T. P. Russell, *Science*, 2003, **299**, 226.
20 J. E. Park, D. R. Hickey, S. Jun, S. Kang, X. Hu, X. J. Chen and S. J. Park, *Adv. Funct. Mater.*, 2016, **26**, 7791–7798.
21 R. Cai, D. Yang, K. T. Lin, Y. Lyu, B. Zhu, Z. He, L. Zhang, Y. Kitamura, L. Qiu, X. Chen, Y. Zhao, Z. Chen and W. Tan, *J. Am. Chem. Soc.*, 2019, **141**, 1725–1734.
22 A. Heuer-Jungemann, N. Feliu, I. Bakaimi, M. Hamaly, A. Alkilany, I. Chakraborty, A. Masood, M. F. Casula, A. Kostopoulou, E. Oh, K. Susumu, M. H. Stewart, I. L. Medintz, E. Stratakis, W. J. Parak and A. G. Kanaras, *Chem. Rev.*, 2019, **119**, 4819–4880.
23 Y. Liu, M. Kim, Y. Wang, Y. A. Wang and X. Peng, *Langmuir*, 2006, **22**, 6341–6345.
24 J. De Roo, Y. Justo, K. De Keukeleere, F. Van den Broeck, J. C. Martins, I. Van Driessche and Z. Hens, *Angew. Chem., Int. Ed.*, 2015, **54**, 6488–6491.
25 K. V. Korpany, D. D. Majewski, C. T. Chiu, S. N. Cross and A. S. Blum, *Langmuir*, 2017, **33**, 3000–3013.
26 X. Hu, C. J. Kim, S. K. Albert and S. J. Park, *Langmuir*, 2018, **34**, 14342–14346.
27 L. Liu, Z. Gao, B. Jiang, Y. Bai, W. Wang and Y. Yin, *Nano Lett.*, 2018, **18**, 5312–5318.
28 M. A. Boles, D. Ling, T. Hyeon and D. V. Talapin, *Nat. Mater.*, 2016, **15**, 141–153.
29 A. Heuer-Jungemann, N. Feliu, I. Bakaimi, M. Hamaly, A. Alkilany, I. Chakraborty, A. Masood, M. F. Casula, A. Kostopoulou, E. Oh, K. Susumu, M. H. Stewart, I. L. Medintz, E. Stratakis, W. J. Parak and A. G. Kanaras, *Chem. Rev.*, 2019, **119**, 4819–4880.
30 K. D. Gatsouli, S. Pispas and E. I. Kamitsos, *J. Phys. Chem. C*, 2007, **111**, 15201–15209.

31 P. Xu, K. Chang, Y. I. Park, B. Zhang, L. Kang, Y. Du, R. S. Iyer and H.-L. Wang, *Polymer*, 2013, **54**, 485–489.
32 S. Lin, W.-L.-J. Hasi, X. Lin, S.-Q.-G.-W. Han, X.-T. Lou, F. Yang, D.-Y. Lin and Z.-W. Lu, *Anal. Methods*, 2015, **7**, 5289–5294.
33 C. Yi, Y. Yang, B. Liu, J. He and Z. Nie, *Chem. Soc. Rev.*, 2020, **49**, 465–508.
34 J. Park, K. An, Y. Hwang, J. G. Park, H. J. Noh, J. Y. Kim, J. H. Park, N. M. Hwang and T. Hyeon, *Nat. Mater.*, 2004, **3**, 891–895.
35 J. J. Hao, J. Zhou and C. Y. Zhang, *Chem. Commun.*, 2013, **49**, 6346–6348.
36 O. Chen, J. Zhao, V. P. Chauhan, J. Cui, C. Wong, D. K. Harris, H. Wei, H. S. Han, D. Fukumura, R. K. Jain and M. G. Bawendi, *Nat. Mater.*, 2013, **12**, 445–451.
37 L. Carbone, C. Nobile, M. De Giorgi, F. D. Sala, G. Morello, P. Pompa, M. Hytch, E. Snoeck, A. Fiore, I. R. Franchini, M. Nadasan, A. F. Silvestre, L. Chiodo, S. Kudera, R. Cingolani, R. Krahne and L. Manna, *Nano Lett.*, 2007, **7**, 2942–2950.